



# Active Brownian particles in a biased periodic potential

Meng Su<sup>1,a</sup> and Benjamin Lindner<sup>2,3,b</sup>

<sup>1</sup> School of Mathematics and Statistics, Northwestern Polytechnical University, 710129 Xi'an, Shaanxi, People's Republic of China

<sup>2</sup> Department of Physics, Humboldt Universität zu Berlin, Newtonstr 15, 12489 Berlin, Germany

<sup>3</sup> Bernstein Center for Computational Neuroscience, Haus 2, Philippstr 13, 10115 Berlin, Germany

Received 18 November 2022 / Accepted 19 March 2023

© The Author(s), under exclusive licence to EDP Sciences, SIF and Springer-Verlag GmbH Germany, part of Springer Nature 2023

**Abstract** We study transport properties of an active Brownian particle with an Rayleigh–Helmholtz friction function in a biased periodic potential. In the absence of noise and depending on the parameters of the friction function and on the bias force, the motion of the particle can be in a locked state or in different running states. According to the type of solutions, the parameter plane of friction and bias force can be divided into four regions. In these different regimes, there is either only a locked state, only a running state, a bistability between locked and running states, or a bistability of two different running states (corresponding to a systematic motion to the left or right, respectively). In the presence of noise, the mean velocity depends in different ways on the noise intensity for the various parameter regimes. These dependences are explored by means of numerical simulations and simple analytical estimates for limiting cases.

## 1 Introduction

Active Brownian motion can describe self-propelled motion in biology, ranging from vesicles pulled by molecular motors at the subcellular level to the movements of entire cells, of animals and even herds and flocks of animals, see [1–5]. Furthermore, artificial self-propelled particles have been developed [6–10] which can be described in the same mathematical framework. In contrast to a passive Brownian motion, active particles are driven by a source of negative “dissipation,” which can be realized by making the friction coefficient a function of the particle’s speed that becomes negative for small values of the velocity [2, 11]. That is to say, the friction of active Brownian particles acts as an energy pump and dissipation when its coefficient is negative and positive, respectively.

The behavior of active particles in spatially structured environments, specifically in different spatial potentials has been studied in various variants and has been reviewed before, see, e.g., [2]; we just mention the limit-cycle motion of active particles in harmonic potentials [11], the nontrivial effect of a constant bias force on the diffusion properties of active particles [12, 13], the escape rate of active particles out of a metastable potential well [14, 15], and anomalous diffusion for active particles in random environments, e.g., in a Lorentz gas [16–18].

An elementary potential form that has not been studied in the context of active motion is a biased periodic potential, corresponding to a periodic force field. Such a potential has been extensively studied for passive Brownian motion, where it appears in stochastic models of diverse systems such as Josephson junctions [19], phase-locked loops [20], or superionic conduction [21]. Early work on passive motion in inclined periodic potentials includes that by Risken and collaborators [22, 23] and is comprehensively reviewed in his text book [24]. Later studies focused on the diffusion and transport regularity [25–27], on the distinction between overdamped and underdamped motion [28–35], and on experimental realizations [36–39]. For noiseless active particles in a biased periodic potential and under a periodic forcing, the transport characteristics have been studied in [40].

As active motion becomes more and more interesting in diverse scientific fields and a periodic force field is one of the simplest possibilities to create a spatially structured but unbounded environment, we combine here the two model ingredients and study active Brownian particles in a biased periodic potential, focusing on the mean velocity of the particles as the central statistics of interest. We show that the velocity displays a rich dynamics.

Our paper is organized as follows. We first introduce the model for active Brownian particles in a biased periodic potential and the main statistics of interest, the mean long-time velocity used to characterize the transport property of the model. We then consider first the system in the absence of noise and divide the parameter

<sup>a</sup> e-mail: [su\\_mengsm@163.com](mailto:su_mengsm@163.com) (corresponding author)

<sup>b</sup> e-mail: [benjamin.lindner@physik.hu-berlin.de](mailto:benjamin.lindner@physik.hu-berlin.de)

plane of active friction strength and bias force into four regimes according to the type of solutions. In order to elucidate the transport characteristics in the presence of noise, the mean velocity as a function of the noise intensity is shown for the distinct regimes identified previously. In the numerically challenging limit of weak noises, we also investigate the effect of the simulation’s time window and the initial conditions used to estimate the mean velocity. We conclude with a brief summary of our results and an outlook on open problems related to the studied system.

## 2 Model and measures

The equations of motion for active Brownian particles in a biased periodic potential reads

$$\dot{x} = v, \quad m\dot{v} = -\gamma(v)v - \frac{dU}{dx} + \sqrt{2D}\xi(t), \quad (1)$$

where  $U(x) = -u_0 \cos(x) - Fx$  is the biased cosine potential function with bias force  $F$  and  $\xi(t)$  is Gaussian white noise with intensity  $D$  and correlation function  $\langle \xi(t)\xi(t+\tau) \rangle = \delta(\tau)$ . We consider particles with unit mass  $m = 1$  and a potential with unit amplitude  $u_0 = 1$ . The nonlinear friction  $\gamma(v) = \gamma_0(v^2 - v_0^2)$  is the Rayleigh–Helmholtz (RH) friction function [11], in which  $v_0 > 0$  is the speed the particle would reach within a long-time limit if the noise and potential would be omitted. The friction function is negative for  $-v_0 < v < v_0$ . When the velocity of particles is in this range, they are subjected to a negative dissipation, i.e., they are energetically pumped, which results in a self-propelled motion. Here, we consider  $v_0 = 1$ . For  $|F| < 1$ , the potential function has minima at  $x = \arcsin(F) + 2n\pi$ , where  $n$  is an integer. The particle is likely to oscillate around a minimum, escape to another minimum, or keep running through the minima. For  $|F| \geq 1$ , the potential function is monotonically decreasing or increasing. Correspondingly, the velocity can only be in a running state. Since the case for  $F < 0$  is symmetric to that for  $F > 0$ , we only consider positive bias forces.

In the absence of noise, we denote by

$$\bar{v}_{\text{det}} = \lim_{t \rightarrow \infty} \frac{x(t) - x(0)}{t} \quad (2)$$

the time-averaged velocity. If  $\bar{v}_{\text{det}} = 0$ , the particle is captured around a minimum and is in a locked state, whereas non-vanishing values of  $\bar{v}_{\text{det}}$  correspond to the particle running to the right or left.

In the presence of noise, the mean velocity characterizes the long-term properties of Brownian particles as:

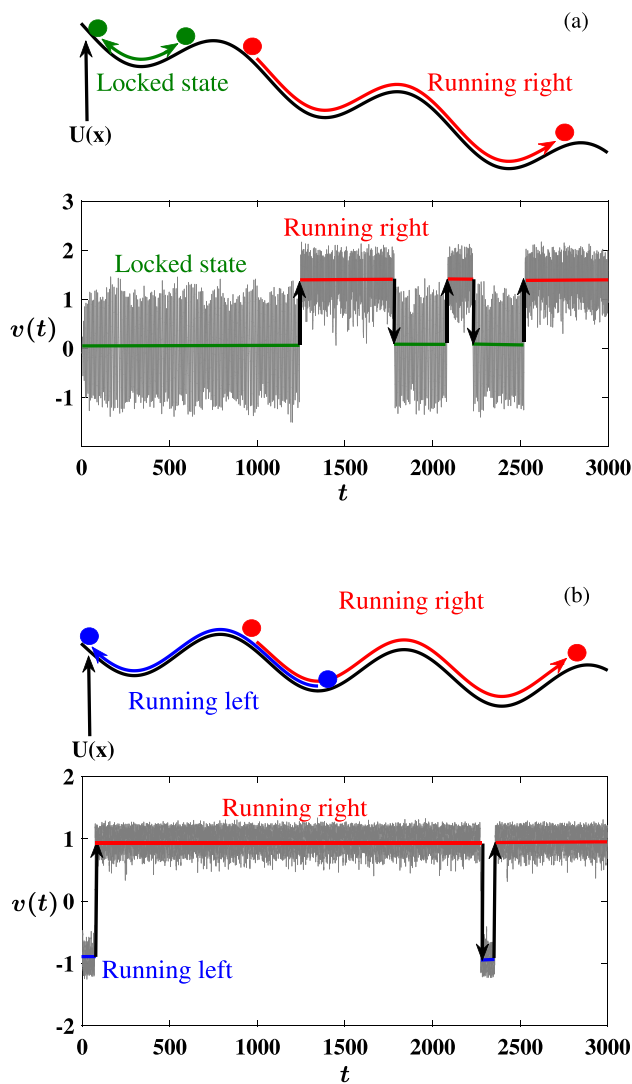


**Fig. 1** Active Brownian particles in a biased periodic potential show diverse velocity dynamics. The particles can not only switch between a locked state (green particle) and running down of the potential hill (red particle) in **a**, but also switch between running to the left (blue particle) and to the right (red particle) in **b**. Examples of transitions (black arrows) between the states are shown in the time series of the velocity. Parameters are  $\gamma_0 = 0.128, F = 0.334$  in **a** and  $\gamma_0 = 3.0, F = 0.1$  in **b**

$$\langle v \rangle = \lim_{t \rightarrow \infty} \frac{\langle x(t) - x(0) \rangle}{t}, \quad (3)$$

where  $\langle \cdot \rangle$  indicates the statistical average over an ensemble of trajectories. In this paper, we focus on the mean velocity as the most important transport property of the active Brownian particle. Equation (1) is integrated with a stochastic Euler–Maruyama scheme [41] with time step  $\Delta t = 10^{-4}$ .

As illustrated in Fig. 1a, the particle cannot only be captured in a local potential minimum but also run down of the potential hill, and in Fig. 1b, transitions between running to the right and left are observed.

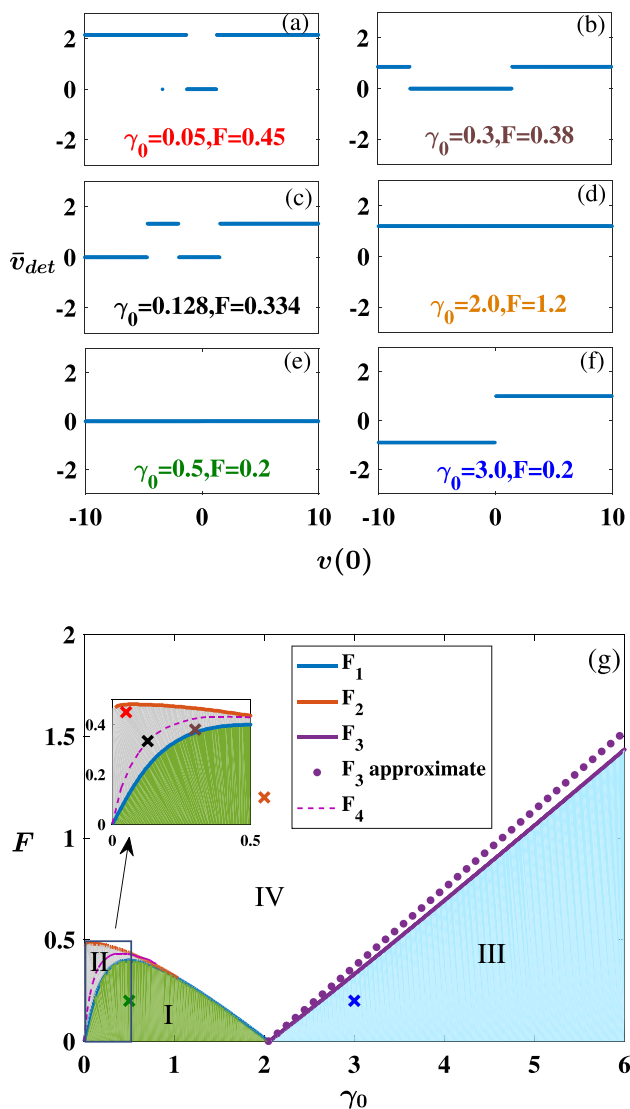


**Fig. 2** The  $(\gamma_0, F)$  plane is divided into four regimes I–IV, as shown in (g), according to the time-averaged velocity  $\bar{v}_{det}$  on the initial velocity. Corresponding examples of  $\bar{v}_{det}$  as a function of initial conditions in the four regions are shown in (a–f), and the locations of the parameters are marked by the crosses with corresponding colors in (g). Bistability can be observed when  $\gamma_0$  and  $F$  are within particular parameter regions (II and III).  $F_1, F_2, F_3, F_4$  are from numerical solutions of the deterministic system; the dotted (approximating) line is obtained analytically

### 3 Transport regimes of the deterministic dynamics

In this section, we consider the system in the absence of noise ( $D = 0$ ). Depending on the choice of parameters and on the initial conditions  $(x(0), v(0))$ , the system may attain one of several possible transport states. We identify the number and nature of the different transport states for one set of system parameters  $(\gamma_0, F)$  by simulating the deterministic system for a large range

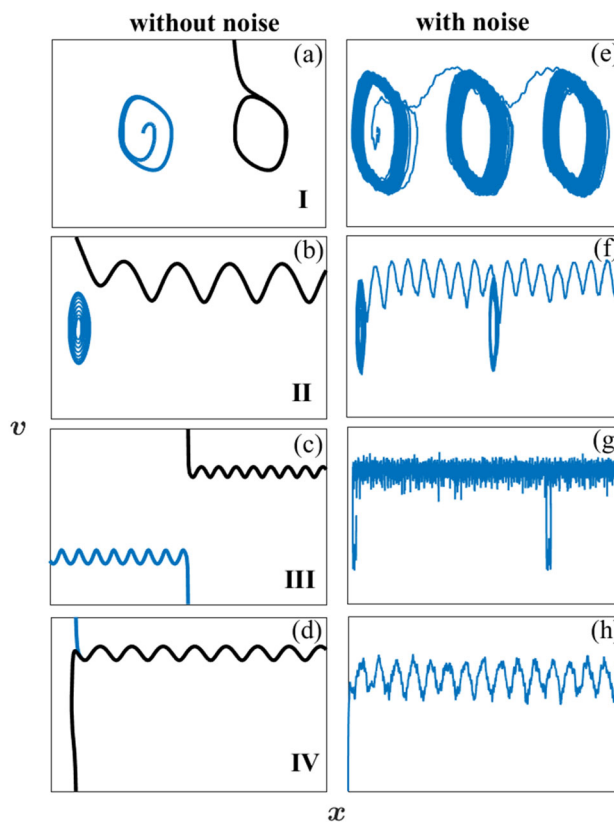


**Fig. 3** Trajectories of the deterministic (a–d) and stochastic (e–h) systems with parameters from the various regimes. The two curves in a–d are the solutions of the deterministic system with the same set of parameters and different initial conditions. Under the same parameters  $(\gamma_0, F)$  and in the presence of weak noise, corresponding phase diagrams are shown in the right hand side. In the locked state area, the particles are likely to overcome the potential hill and vibrate around another potential minimum on the right, as shown in e. In the bistable regimes, transitions between the states take place (f and g)

of initial velocities (the initial position is always picked at the minimum of the potential). This procedure is illustrated in Fig. 2a–f and reveals different transport regimes, as shown in Fig. 2g.

In the green area, for sufficiently small bias and small  $\gamma_0$ , the particle is constrained to the potential minimum and approaches a limit cycle (locked state). Different initial conditions may lead to different limit cycles belonging to different minima of the periodic potential (two distinct limit cycles are shown in Fig. 3a), all possessing vanishing time-averaged velocity,  $\bar{v}_{det} = 0$ . Take  $\gamma_0 = 0.5, F = 0.2$  in the locked state area as an example: Fig. 2e shows that the function  $\bar{v}_{det}$  is zero for all initial velocities  $v(0)$ .

In the gray and light blue areas, two types of bistability can be observed. One type of bistability is encountered at very small friction coefficient and for a bias force in the range

$$F_1(\gamma_0) < F < F_2(\gamma_0), \tag{4}$$

here the particle is either in the locked state or runs to the right, i.e., in the direction of the bias force. Accordingly, the time-averaged velocity attains two different values depending on the initial velocity (see examples in Fig. 2a–c and different types of trajectories in Fig. 3b). The entire region of forces and friction coefficients for which this bistability is observed is shown as the gray-shaded area in Fig. 2g.

When the friction parameter  $\gamma_0$  is large enough, the particle can attain sufficient energy to overcome dissipative losses and climb up the potential hill. If the parameter of the active friction function exceeds a critical value,  $\gamma_0 > \gamma_{0,c} \approx 2.05$ , the other type of bistability is observed when

$$F < F_3(\gamma_0), \tag{5}$$

which is marked as the light blue area. The trajectory either runs to the right or to the left, as shown in Fig. 2f for  $\bar{v}_{\text{det}}(v(0))$  and in Fig. 3c for the trajectories running in different directions.

In the remaining white area, only one running state can be observed. When the parameters are in this range, no matter what the initial velocity is, the particle will eventually run to the right. We note that for no parameter combination with  $\gamma_0 > 0$  we will be able to observe more than two stable states.

The slope of  $F_3(\gamma_0)$  in Fig. 2g can be analytically estimated based on a simplifying assumption. In the absence of noise,

$$-\gamma_0(v^2 - 1)v - \sin(x) + F = 0 \tag{6}$$

determines the nullcline for the variable  $v$ . When the friction parameter is large, we can assume that both the active friction term and the force are large compared to  $\sin(x)$  and we can neglect the latter term. This leads to a cubic equation in  $v$ , reading  $(v^2 - 1)v = F/\gamma_0$ , which has one, two, or three solutions depending on  $F/\gamma_0$ . If there are three solutions, the upper and lower solutions are stable, while the middle one is unstable in  $v$ . The critical value for  $F/\gamma_0$  is  $2/3\sqrt{3}$ , which is the slope of the dotted line in Fig. 2g (note that there is also an offset in the critical force  $F_3(\gamma_0)$  that we do not account for).

Returning to the first kind of bistability between locked and running states, the gray region can be further divided by the dashed line into regions in which the locked or the running state is more stable, in the zero noise intensity limit. As an approximate way to determine this line, we use stochastic simulations for a small noise intensity of  $D = 0.005$  to find this critical force with the help of the distributions of the time-averaged velocity. For a parameter set  $\gamma_0, F$  for which the velocity’s probability density has a strong peak around  $v = 0$  (with the integrated probability of the peak being larger than 1/2), the locked state is the more stable state. The opposite is true if the density of the velocity has a strong peak at a non-vanishing value.

We note that if we plot the probability density of the *instantaneous* velocity, the peaks do not become

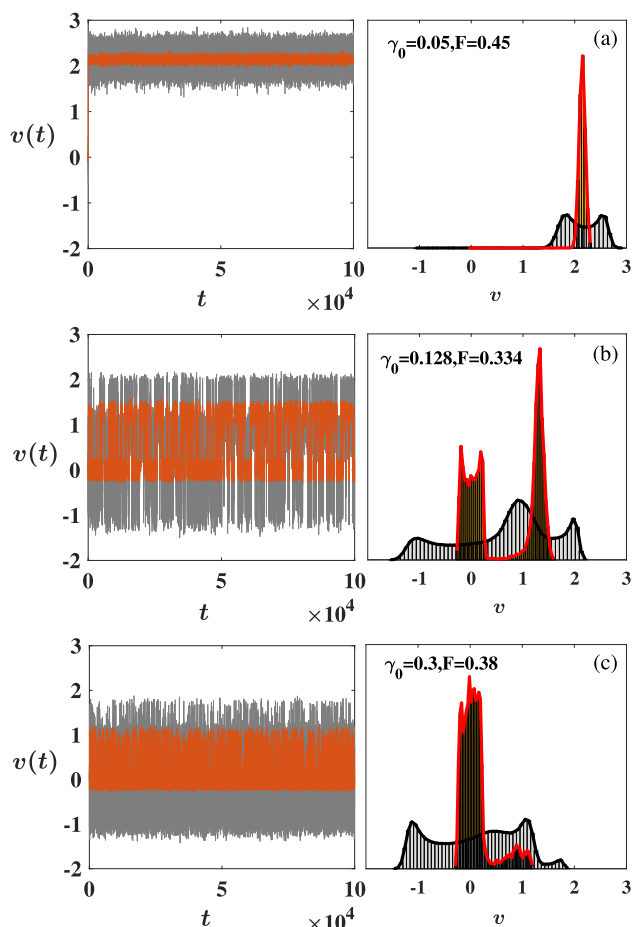


**Fig. 4** The gray area can be further divided into regions above and below the dashed line in Fig. 2g [close-up in the inset], in which the running or locked state is more stable in the zero noise intensity limit. Corresponding time series and distributions of the original (gray) and time-averaged velocities (orange) for  $D = 0.005$  are compared, in which the parameters in **a** and **c** are from the regions that running state and locked state are more stable, respectively. The set of parameters in **b** is close to the critical curve

apparent but can show more than one peak both in the locked state (because the active particle undergoes a limit-cycle motion similar to that observed in a harmonic potential [11]) and in the running state (because the motion along the inclined periodic potentials undergoes periods of faster and of slower motion depending on the spatial region). Two peaks in the running state can be also observed for some parameter values for a passive Brownian particle in a harmonic potential and have been referred to as multistability (as opposed to a mere bistability) of the stochastic dynamics [35, 42], but we think that this is a misnomer, both in the case of passive motion and also for the active motion in periodic potentials considered here. The so-called multistability in the running state would be even observed in the absence of noise when the system systematically passes back and forth between the two states. These “states” (i.e., the velocities where the probability density dis-



plays maxima) are neither stable nor metastable in the sense that without a sufficiently strong perturbation the state would be attained for an infinite time<sup>1</sup>.

Instead of the instantaneous velocity, it is more meaningful for the long-term transport characteristics of the system to consider histograms of velocities that are time averaged over a suitable time window (a similar averaging has been used in the case of passive Brownian motion in a biased periodic potential for the running state [35]). The distributions of the original and time-averaged velocity are compared in Fig. 4. When choosing the time bin as 10 to obtain the time-averaged trajectories, the main share of probability is located in two ranges of velocities with a minimum in between—this minimum can be regarded as the boundary that divides the locked and running states for a certain set of parameters. For a fixed friction coefficient  $\gamma_0$ , equal probabilities on each side of the boundary determine the critical force  $F_4$ .

In order to illustrate the above, we show in Fig. 4 the velocity distributions for the original (gray) and time-averaged velocities (orange) for three sets of parameters. At  $\gamma_0 = 0.05, F = 0.45$  (Fig. 4a) and  $\gamma_0 = 0.3, F = 0.38$  (Fig. 4c), the running or the locked state is more stable, respectively. The parameter set  $\gamma_0 = 0.128, F = 0.334$  (Fig. 4b) is on the critical curve, i.e., here the probabilities to be in the locked and running state are approximately equal when  $D = 0.005$ . We indicate the locations of these parameter sets by crosses in Fig. 2g.

### 4 Mean velocity in the presence of noise

We now inspect how the mean velocity depends on the intensity  $D$  of the uncorrelated fluctuations in the distinct transport regimes discussed in the previous section.

For different parameter sets  $\gamma_0, F$ , Fig. 5 shows the mean velocity vs the noise intensity  $D$ . When estimating the long-term mean velocity from simulations, it is important to keep in mind that the time window  $T$  should be large enough; we use  $T = 10^5$  in Fig. 5 but will discuss the role of the time window below. The number of realizations to calculate the mean velocity is  $10^3$ .

One limit case is rather simple: When the noise becomes stronger and stronger, the mean velocity converges to zero. In this limit, the modulation of the force by the periodic part of the potential can be neglected (but not the systematic bias) and the effective dynamics approaches the form

<sup>1</sup> As an example consider a limit-cycle motion in a two-dimensional system which projected on one coordinate displays a bimodal distribution in the time-averaged density (e.g., the two peaks associated with the locked state in Fig. 4c). It does not seem reasonable to interpret the bimodality of the probability density as an indication of a bistability of the dynamics, which only reflects the speed with which the system proceeds along the limit cycle.

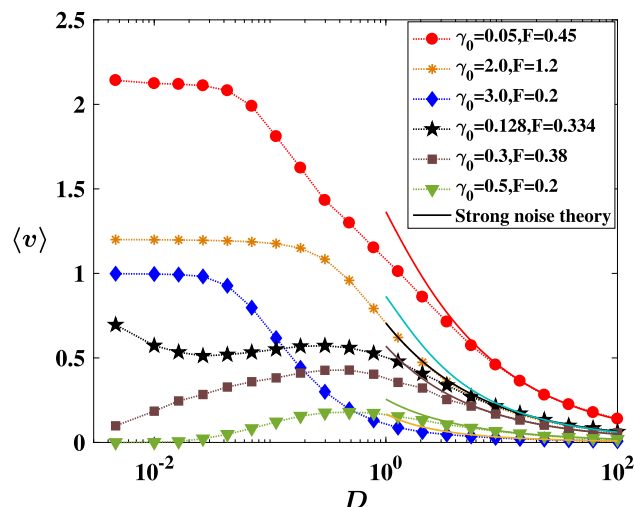


**Fig. 5** Mean velocities versus noise intensity for  $\gamma_0$  and  $F$  in different regimes. The solid lines represent the mean velocity in theory for strong noise, i.e.,  $\langle v \rangle_{sn} = \int_{-\infty}^{+\infty} dv P_0(v)v$ , where  $P_0(v)$  is given in Eq. (9). The dotted lines with symbols are results of numerical simulations

$$\dot{v} = -\gamma(v)v + F + \sqrt{2D}\xi(t). \tag{7}$$

The corresponding Fokker–Planck equation for the velocity variable

$$\partial_t P(v, t) = \partial_v [\gamma(v)v - F + D\partial_v] P(v, t) \tag{8}$$

has a simple stationary solution ( $\partial_t P_0(v) = 0$ ):

$$P_0(v) = \frac{\exp\left[-\frac{\gamma_0 v^4/4 - \gamma_0 v_0^2 v^2/2 - Fv}{D}\right]}{\int_{-\infty}^{+\infty} d\tilde{v} \exp\left[-\frac{\gamma_0 \tilde{v}^4/4 - \gamma_0 v_0^2 \tilde{v}^2/2 - F\tilde{v}}{D}\right]}. \tag{9}$$

The mean value of this distribution,  $\langle v \rangle_{sn} = \int_{-\infty}^{+\infty} dv P_0(v)v$ , indeed tends to zero as  $D \rightarrow \infty$  (solid lines in Fig. 5) and generally agrees well with our simulation results for large but finite  $D$  (for a discussion of this asymptotic behavior, see [43]). We note that this limiting behavior is very different to the behavior of a passive Brownian particle in an inclined periodic potential for which the mean velocity would approach  $\langle v \rangle_{sn} = F/\gamma$  [44], where  $\gamma$  is the Stokes friction coefficient.

If the parameters  $\gamma_0$  and  $F$  are in the regime of the locked state ( $\gamma_0 = 0.5, F = 0.2$ ), the mean velocity first increases, attains a maximum at intermediate noise level, and then decreases as already discussed above. The initial increase of the mean velocity is due to the fact that, with noise, the particles get a chance to repeatedly overcome the potential barriers to the right (see Fig. 3e).

For parameters in the running regime ( $\gamma_0 = 2.0, F = 1.2$ ), the mean velocity as a function of  $D$  first remains flat, i.e., the velocity does not depend on the noise, and then decreases monotonically. The initial constant value

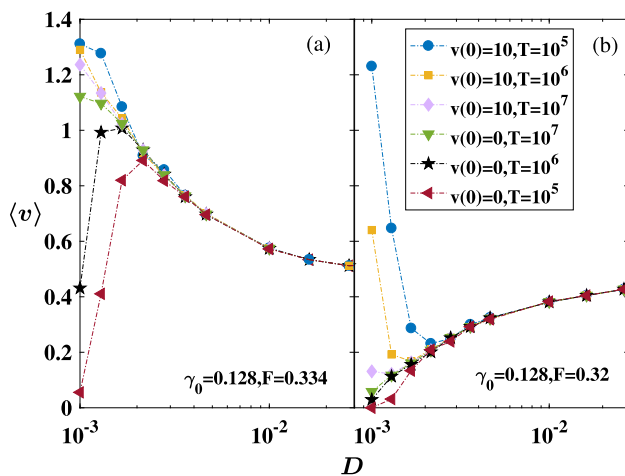


**Fig. 6** Effects of the time window  $T$  and initial velocity  $v(0)$  used to estimate the mean velocity under weak noises. When  $v(0) = 0$  and  $10$ , the particle starts from the locked or running state, respectively

corresponds to the deterministic speed, Eq. (2), and has been found for the parameter set in Fig. 2d.

When the parameters are in the regime of bistability of running to the left or to the right (light blue area in Fig. 2g), we observe a monotonic decrease of the velocity with growing noise intensity. In the zero noise limit, the system attains the more stable velocity which for  $F > 0$  is the positive one (cf the upper branch in Fig. 2f). Additional noise makes the second (negative) velocity state also somewhat more likely and thus reduces the mean velocity.

The two parameter sets  $\gamma_0 = 0.05, F = 0.45$  and  $\gamma_0 = 0.3, F = 0.38$  are both in the other bistable regime (gray area in Fig. 2g) where the locked state and a running state coexist. The two sets differ with respect to the dominating stability of the two states (determined by the histogram method discussed in the previous section): For  $\gamma_0 = 0.05, F = 0.45$ , the running state is more stable, whereas for  $\gamma_0 = 0.3, F = 0.38$ , the locked state is more stable. The dependence of the mean velocity on the noise intensity is qualitatively different for these two cases. If the running state is more stable, the mean velocity monotonically decreases with  $D$ , similar to the case of the running regime discussed above. If the locked state is more stable, we obtain a nonmonotonic curve with a clear maximum, similar to the case of the locked regime.

Close to the critical line which subdivides the bistable area of locked and running states, the dependence of the mean velocity on  $D$  becomes more complicated over the entire range of noise levels. For  $\gamma_0 = 0.128, F = 0.334$  (black stars in Fig. 5), the mean velocity first decreases to a minimum, then increases, passes through a maximum, and finally decays to zero.

At weak noise, the time window  $T$  and initial condition of the velocity  $v(0)$  used to estimate the mean velocity will become important such that the mean velocity may strongly depend on the initial condition as

long as we cannot simulate the system for an extremely long time. In particular, when the parameters are close to the critical curve in the bistable regime and the noise intensity is small, the mean velocity (determined via a time average) depends strongly on the initial state of the particle. If we start the particle in the running state, then, irrespective of whether the running state is more stable (Fig. 6a) or the locked state is more stable (Fig. 6b), the mean velocity at low noise is high. If we start the particle in the locked state on the contrary, the mean velocity is very small. Independence on initial conditions requires larger and larger averaging time windows for decreasing values of the noise intensity, as illustrated in Fig. 6.

## 5 Summary

In this paper, we have studied the transport properties of active Brownian particles in a biased periodic potential. For the noiseless system ( $D = 0$ ), we have identified qualitatively distinct transport regimes with different numbers of stable states of the particle's velocity: a purely running state, a locked state, a bistable regime with two running states, and finally another bistable regime with a running and a locked state. For all these regimes, we have explored the noise dependence of the mean velocity. The existence of the distinct stable states of the particle's velocity as well as noise-induced transitions between these states can also be observed when other variants of the active Brownian particle are used, for instance, the active friction model by Schweitzer, Ebeling, and Tilch (not shown). In this sense, our results do not hinge on the fine details of the active particle model.

If the system is dominated by a running state, either because it is the only stable state or it is the more probable state, the mean velocity decreases with increasing noise intensity and can be captured for strong noise by our approximation Eq. (9). The decrease of the mean velocity to zero in the strong noise limit is a nontrivial result in marked contrast to the passive Brownian motion in a biased periodic potential [24, 44]. If the system is dominated by the locked state, the velocity displays a nonmonotonic dependence on the noise intensity; it vanishes for both  $D \rightarrow 0$  and  $D \rightarrow \infty$ . Consequently, there is an optimal noise that maximizes the velocity. Close to the critical line of equal probability for the locked and the running state, the velocity as a function of  $D$  can become more complicated, attaining a minimum and a maximum at finite values of  $D$ .

Here, we have focused on the mean velocity as the sole characteristic of transport. In many applications, however, also the regularity of transport is of interest. This can be quantified by the Péclet number or by the diffusion coefficient of the particles (see, for instance, [25, 44, 45]). While the diffusion of passive particles in a biased periodic potential is a well-studied subject [24–26, 33, 44], there is nothing known to our knowledge about the diffusion coefficient of active particles in such

a potential. This constitutes an interesting problem for future research.

## Author contribution statement

The authors declare equal contributions.

**Data availability** The data that support the findings of this study are available from the corresponding author upon reasonable request.

## Declarations

**Conflict of interest** The authors declare no conflict of interests.

## References

1. D. Bray, *Cell Movements: From Molecules to Motility* (Garland Science, New York, 2000)
2. P. Romanczuk, M. Bär, W. Ebeling, B. Lindner, L. Schimansky-Geier, Active Brownian particles. *Eur. Phys. J. Spec. Top.* **202**(1), 1–162 (2012). <https://doi.org/10.1140/epjst/e2012-01529-y>
3. J. Elgeti, R.G. Winkler, G. Gompper, Physics of microswimmers—single particle motion and collective behavior: a review. *Rep. Prog. Phys.* **78**(5), 056601 (2015). <https://doi.org/10.1088/0034-4885/78/5/056601>
4. C. Bechinger, R. Di Leonardo, H. Löwen, C. Reichhardt, G. Volpe, G. Volpe, Active particles in complex and crowded environments. *Rev. Mod. Phys.* **88**(4), 045006 (2016). <https://doi.org/10.1103/RevModPhys.88.045006>
5. S. Henkes, K. Kostanjevec, J.M. Collinson, R. Sknepnek, E. Bertin, Dense active matter model of motion patterns in confluent cell monolayers. *Nat. Commun.* **11**(1), 1–9 (2020). <https://doi.org/10.1038/s41467-020-15164-5>
6. W.F. Paxton, K.C. Kistler, C.C. Olmeda, A. Sen, S.K. St. Angelo, Y. Cao, T.E. Mallouk, P.E. Lammert, V.H. Crespi, Catalytic nanomotors: autonomous movement of striped nanorods. *J. Am. Chem. Soc.* **126**(41), 13424–13431 (2004). <https://doi.org/10.1021/ja047697z>
7. J.R. Howse, R.A. Jones, A.J. Ryan, T. Gough, R. Vafabakhsh, R. Golestanian, Self-motile colloidal particles: from directed propulsion to random walk. *Phys. Rev. Lett.* **99**(4), 048102 (2007). <https://doi.org/10.1103/PhysRevLett.99.048102>
8. R. Kapral, Perspective: Nanomotors without moving parts that propel themselves in solution. *J. Chem. Phys.* **138**(2), 020901 (2013). <https://doi.org/10.1063/1.4773981>
9. M. Schmitt, H. Stark, Active Brownian motion of emulsion droplets: coarsening dynamics at the interface and rotational diffusion. *Eur. Phys. J. E* **39**(8), 1–15 (2016). <https://doi.org/10.1140/epje/i2016-16080-y>
10. A. Chamolly, E. Lauga, Stochastic dynamics of dissolving active particles. *Eur. Phys. J. E* **42**(7), 1–15 (2019). <https://doi.org/10.1140/epje/i2019-11854-3>
11. U. Erdmann, W. Ebeling, L. Schimansky-Geier, F. Schweitzer, Brownian particles far from equilibrium. *Eur. Phys. J. B* **15**(1), 105–113 (2000). <https://doi.org/10.1007/s100510051104>
12. B. Lindner, E.M. Nicola, Critical asymmetry for giant diffusion of active Brownian particles. *Phys. Rev. Lett.* **101**(19), 190603 (2008). <https://doi.org/10.1103/PhysRevLett.101.190603>
13. C. Touya, T. Schwalger, B. Lindner, Relation between models of cooperative molecular motors and active Brownian particles. *Phys. Rev. E.* **83**, 051913 (2011). <https://doi.org/10.1103/PhysRevE.83.051913>
14. P.S. Burada, B. Lindner, Escape rate of an active Brownian particle over a potential barrier. *Phys. Rev. E.* **85**, 032102 (2012). <https://doi.org/10.1103/PhysRevE.85.032102>
15. A. Militaru, M. Innerbichler, M. Frimmer, F. Tebbenjohanns, L. Novotny, C. Dellago, Escape dynamics of active particles in multistable potentials. *Nat. Commun.* **12**(1), 1–6 (2021). <https://doi.org/10.1038/s41467-021-22647-6>
16. M. Zeitz, K. Wolff, H. Stark, Active Brownian particles moving in a random lorentz gas. *Eur. Phys. J. E* **40**(2), 1–10 (2017). <https://doi.org/10.1140/epje/i2017-11510-0>
17. O. Chepizhko, E.G. Altmann, F. Peruani, Optimal noise maximizes collective motion in heterogeneous media. *Phys. Rev. Lett.* **110**(23), 238101 (2013). <https://doi.org/10.1103/PhysRevLett.110.238101>
18. O. Chepizhko, F. Peruani, Diffusion, subdiffusion, and trapping of active particles in heterogeneous media. *Phys. Rev. Lett.* **111**(16), 160604 (2013). <https://doi.org/10.1103/PhysRevLett.111.160604>
19. L. Longobardi, D. Massarotti, G. Rotoli, D. Stornaiuolo, G. Papari, A. Kawakami, G.P. Pepe, A. Barone, F. Tafuri, Thermal hopping and retrapping of a Brownian particle in the tilted periodic potential of a nbn/mgo/nbn josephson junction. *Phys. Rev. B.* **84**, 184504 (2011). <https://doi.org/10.1103/PhysRevB.84.184504>
20. R.L. Stratonovich, *Topics in the Theory of Random Noise* (Gordon and Breach, New York, 1967)
21. P. Fulde, L. Pietronero, W.R. Schneider, S. Strässler, Problem of Brownian motion in a periodic potential. *Phys. Rev. Lett.* **35**, 1776 (1975). <https://doi.org/10.1103/PhysRevLett.35.1776>
22. H. Vollmer, H. Risken, Eigenvalues and their connection to transition rates for the Brownian motion in an inclined cosine potential. *J. Phys. B Cond. Mat.* **52**, 259 (1983). <https://doi.org/10.1007/BF01307378>
23. P. Jung, H. Risken, Eigenvalues for the extremely underdamped Brownian motion in an inclined periodic potential. *Z. Phys. B. Con. Mat.* **54**, 357 (1984). <https://doi.org/10.1007/BF01485833>
24. H. Risken, *The Fokker-Planck Equation* (Springer, Berlin, 1984)
25. B. Lindner, M. Kostur, L. Schimansky-Geier, Optimal diffusive transport in a tilted periodic potential. *Fluct. Noise Lett.* **1**, R25 (2001). <https://doi.org/10.1142/S0219477501000056>
26. P. Reimann, C. Van den Broeck, H. Linke, P. Hänggi, J.M. Rubi, M.A. Pérez-Madrid, Giant acceleration of free diffusion by use of tilted periodic potentials. *Phys. Rev. Lett.* **87**, 010602 (2001). <https://doi.org/10.1103/PhysRevLett.87.010602>

27. P. Reimann, C. Van den Broeck, H. Linke, P. Hänggi, J.M. Rubi, A. Pérez-Madrid, Diffusion in tilted periodic potentials: enhancement, universality, and scaling. *Phys. Rev. E* **65**, 031104 (2002). <https://doi.org/10.1103/PhysRevE.65.031104>
28. G. Costantini, F. Marchesoni, Threshold diffusion in a tilted washboard potential. *Europhys. Lett.* **48**(5), 491 (1999). <https://doi.org/10.1209/epl/i1999-00510-7>
29. K. Lindenberg, A.M. Lacasta, J.M. Sancho, A.H. Romero, Transport and diffusion on crystalline surfaces under external forces. *New J. Phys.* **7**, 29 (2005). <https://doi.org/10.1088/1367-2630/7/1/029>
30. K. Lindenberg, J.M. Sancho, A.M. Lacasta, I.M. Sokolov, Dispersionless transport in a washboard potential. *Phys. Rev. Lett.* **98**, 020602 (2007). <https://doi.org/10.1103/PhysRevLett.98.020602>
31. J.M. Sancho, A.M. Lacasta, The rich phenomenology of Brownian particles in nonlinear potential landscapes. *Eur. Phys. J. Spec. Top.* **187**, 49 (2010). <https://doi.org/10.1140/epjst/e2010-01270-7>
32. I.G. Marchenko, I.I. Marchenko, Diffusion in the systems with low dissipation: Exponential growth with temperature drop. *Epl-Europhys. Lett.* **100**, 50005 (2012). <https://doi.org/10.1209/0295-5075/100/50005>
33. B. Lindner, I. Sokolov, Giant diffusion of underdamped particles in a biased periodic potential. *Phys. Rev. E* **93**, 042106 (2016). <https://doi.org/10.1103/PhysRevE.93.042106>
34. L.P. Fischer, P. Pietzonka, U. Seifert, Large deviation function for a driven underdamped particle in a periodic potential. *Phys. Rev. E* **97**(2), 022143 (2018). <https://doi.org/10.1103/PhysRevE.97.022143>
35. J. Spiechowicz, J. Luczka, Arcsine law and multistable Brownian dynamics in a tilted periodic potential. *Phys. Rev. E* **104**(2), 024132 (2021). <https://doi.org/10.1103/PhysRevE.104.024132>
36. S.H. Lee, D.G. Grier, Giant colloidal diffusivity on corrugated optical vortices. *Phys. Rev. Lett.* **96**, 190601 (2006). <https://doi.org/10.1103/PhysRevLett.96.190601>
37. M. Evstigneev, O. Zvyagolskaya, S. Bleil, R. Eichhorn, C. Bechinger, P. Reimann, Diffusion of colloidal particles in a tilted periodic potential: theory versus experiment. *Phys. Rev. E* **77**, 041107 (2008). <https://doi.org/10.1103/PhysRevE.77.041107>
38. S. Albaladejo, M.I. Marqués, F. Scheffold, J.J. Sáenz, Giant enhanced diffusion of gold nanoparticles in optical vortex fields. *Nano Lett.* **9**, 3527 (2009). <https://doi.org/10.1021/nl901745a>
39. R. Hayashi, K. Sasaki, S. Nakamura, S. Kudo, Y. Inoue, H. Noji, K. Hayashi, Giant acceleration of diffusion observed in a single-molecule experiment on F1-ATPase. *Phys. Rev. Lett.* **114**(24), 248101 (2015). <https://doi.org/10.1103/PhysRevLett.114.248101>
40. W. Guo, L. Du, Z. Liu, H. Yang, D. Mei, Uphill anomalous transport in a deterministic system with speed-dependent friction coefficient. *Chin. Phys. B* **26**(1), 010502 (2017). <https://doi.org/10.1088/1674-1056/26/1/010502>
41. P.E. Kloeden, E. Platen, *Stochastic Differential Equations* (Springer, Berlin, 1992)
42. J. Spiechowicz, J. Luczka, Diffusion in a biased washboard potential revisited. *Phys. Rev. E* **101**(3), 032123 (2020). <https://doi.org/10.1103/PhysRevE.101.032123>
43. B. Lindner, E.M. Nicola, Diffusion in different models of active Brownian motion. *Eur. Phys. J. Spec. Top.* **157**, 43 (2008). <https://doi.org/10.1140/epjst/e2008-00629-7>
44. P. Reimann, Brownian motors: noisy transport far from equilibrium. *Phys. Rep.* **361**, 57 (2002). [https://doi.org/10.1016/S0370-1573\(01\)00081-3](https://doi.org/10.1016/S0370-1573(01)00081-3)
45. B. Lindner, L. Schimansky-Geier, Noise-induced transport with low randomness. *Phys. Rev. Lett.* **89**, 230602 (2002). <https://doi.org/10.1103/PhysRevLett.89.230602>

Springer Nature or its licensor (e.g. a society or other partner) holds exclusive rights to this article under a publishing agreement with the author(s) or other rightsholder(s); author self-archiving of the accepted manuscript version of this article is solely governed by the terms of such publishing agreement and applicable law.